

# Constant-Optic-Flow Lunar Landing: Optimality and Guidance

Dario Izzo,\* Nicolás Weiss,† and Tobias Seidl‡  
 ESA, 2201 AZ Noordwijk, The Netherlands

DOI: 10.2514/1.52553

Neuromorphic architectures to robust and adaptive navigation based on visual clues have been proposed as automated landing systems. In particular, constant-optic-flow descents have been studied in relation to their bioinspired nature and to their promise for a substantial hardware and software simplification. The main body of work on the topic considers Earth-based systems as applications, such as micro air vehicles, and has only lately looked at planetary landings, but never in relation to their mass optimality. In this paper, constant-optic-flow descents are studied with respect to optimality, first from a theoretical point of view using Pontryagin's maximum principle and then performing a numerical investigation on some selected cases (Apollo-like) and a comparison with unconstrained descents. The propellant mass introduced by forcing a constant optic flow during a lunar descent is estimated for typical high-gate/low-gate conditions. The effect of constraining the spacecraft pitch law during the constant-optic-flow descent is also studied, showing that an optimal pitch law is essential to lower the overall mass consumption and that linear or exponential laws may not be adequate. A guidance algorithm is then presented and discussed for use in automated planetary landing when a constant optic flow is regulated.

## Nomenclature

$\mathbf{b}$	=	boundary constraints
$g$	=	planetary gravity, m/s <sup>2</sup>
$g_0$	=	Earth gravity, m/s <sup>2</sup>
$\mathcal{H}$	=	Hamiltonian
$I_{sp}$	=	specific impulse, s
$m$	=	spacecraft mass, kg
$\mathbf{p}$	=	path constraints
$T$	=	maximum thrust levels, N
$t$	=	time, s
$\mathcal{U}$	=	control space
$u, \tilde{u}$	=	control variables
$\mathbf{u}$	=	control
$v_x$	=	horizontal velocity, m/s
$v_z$	=	vertical velocity, m/s
$x$	=	horizontal range, m
$\mathbf{x}$	=	state
$z, h$	=	height, m
$\beta$	=	spacecraft pitch angle, rad
$\Delta P$	=	relative propellant mass penalty, %
$\Delta \mathbf{U}$	=	impulsive control
$\lambda$	=	costate
$\phi$	=	uncontrolled dynamics
$\chi$	=	elementary motion-detector optic flow reading, V
$\omega$	=	spacecraft angular velocity, rad/s
$\varpi$	=	optic flow, rad/s

## Subscripts

$f$	=	final
$t$	=	target
$0$	=	initial

## Superscripts

$m$	=	middle point
*	=	optimal

## I. Introduction

INSECT flight has been a profound source of inspiration to engineers for the development of lightweight robust guidance and navigation architectures for flying vehicles. Recent research proposes accurate models for the flight of widely studied insects such as the fruit fly *Drosophila melanogaster* [1], bioinspired navigation frameworks for use in micro air vehicles (MAVs) operating in urban environments [2], or complete control architectures for the automated guidance of aircraft based on elementary motion detectors (EMDs) [3]. Some works also investigated the possibility of using similar approaches for the control of MAVs operating on a Mars environment, such as the studies on the Entomopter [4] or the DelFly [5]. The main advantage claimed by these works is simplicity, which typically leads to low-power and low-mass systems. Less attention has been devoted to applications such as spacecraft landing, where visual guidance and navigation techniques proposed are often based on processing images coming from cameras and digital elevation model matching using optical correlators [6]. It seems logical to assume that bioinspired techniques are less attractive if applied to control a spacecraft. A spacecraft is a system that needs to expel mass to accelerate, while no biological systems exploit the principle of reaction engines for locomotion. Nevertheless, the simplicity of some of the bioinspired systems developed is very attractive and motivated some recent studies at ESA [7,8] aimed to study a fully automated guidance and navigation landing systems for lunar and Mars scenarios based on the biological principles (i.e., EMDs and constant optic flow) originally implemented in a different context for MAVs guidance and navigation. In their work the authors focused on the overall architecture, neglecting the optimality of the resulting trajectories with respect to mass. As a consequence, the resulting simulations, although proving the possibility of having a much simplified system for spacecraft landing, did point toward an excessive mass expenditure.

In this paper those results are improved and complemented by an in-depth analysis of constant-optic-flow planetary landings from a mass-optimality standpoint. Optimal descents are produced that present reasonable mass consumptions. The paper is organized as follows: In Sec. II the neuromorphic approach to detect optic flow and the results from Srinivasan et al. [9] are introduced and suggest constant-optic-flow descent strategies for planetary applications. In

Received 27 September 2010; revision received 28 March 2011; accepted for publication 13 April 2011. Copyright © 2011 by Dario Izzo. Published by the American Institute of Aeronautics and Astronautics, Inc., with permission. Copies of this paper may be made for personal or internal use, on condition that the copier pay the \$10.00 per-copy fee to the Copyright Clearance Center, Inc., 222 Rosewood Drive, Danvers, MA 01923; include the code 0731-5090/11 and \$10.00 in correspondence with the CCC.

\*Advanced Concepts Team, European Space Research and Technology Centre, Keplerlaan 1; dario.izzo@esa.int.

†Currently Ph.D. Candidate, Technical University of Delft, Keplerlaan 1, Delft, The Netherlands.

‡Professor, University of Applied Sciences of Gelsenkirchen, Bocholt, Germany.

Sec. III Pontryagin's maximum principle is used to study the optimal control structure of constant-optic-flow descent trajectories in a simple dynamics case, and the lunar landing test case used as a reference in most of the remaining sections is introduced. To allow for an extensive and efficient numerical study, a direct numerical method to solve the optimal control problem is explained in Sec. IV. In the following Sec. V such a direct method is used to compare constant-optic-flow descents with optimal descents and to investigate the influence of constraining suboptimal pitch laws on constant-optic-flow trajectories. Finally, in Sec. VI, a modification is proposed to the original Apollo's guidance algorithm [10] to regulate a constant optic flow during a lunar descent.

## II. Neuromorphic Approach

Neuromorphic electronics [11] mimic neurobiological circuits with the aim of replicating a certain biological model function in a prosthetic or purely technical device. These circuits are realized in analog, digital, or mixed-analog/digital electronics in very-large-scale integration systems. Their major feature is a fault- and noise-tolerant processing of data with minimum processing time while requiring only minimal energy and, consequently, minimal weight and volume. The feature of low power consumption enables the processing of highly parallel data, needed for the auditory and visual systems. In consequence neuromorphic systems find application in diverse scenarios where their features are key requirements, e.g., internal prosthetic cochlea in a human ear [12] or visual control of unmanned aerial vehicles (UAVs). For this last application, research on the visual autopilot of flying insects dates far back into the 1960s aiming at exploiting EMDs, the smallest possible neural circuit able to detect motion of a visual contrast and thus allowing a well-designed array of optical sensors to extract behaviorally relevant features [13]. The findings on EMDs and their subsequent wiring are replicated in electronics, both to validate the biological data and for application in Earthbound UAVs [14–17]. A similar approach to landing has been mentioned in the context of planetary exploration [18], but detailed studies have only recently been performed by the Advanced Concepts Team of ESA and in collaboration with the European academia [7], showing that EMDs are indeed able to detect optic flow information during a planetary landing sequence and can be used in a closed-loop automated landing control system [8]. In these last studies, simulated images from the software PANGU [19] were employed to generate realistic inputs to the sensor and thus evaluate the optic flow. As an example, in Fig. 1b the simulated EMD readings (the EMD model was provided as a courtesy of the University of Marseille [14]) are presented during a spiral descent on a randomly generated asteroid. The orbital angular velocity is kept constant during the descent. The light conditions in the simulation are assumed to be constant, and PANGU [19] is used to simulate the

image input to the sensor, which is assumed to be always pointing at nadir (Fig. 1a shows the simulated asteroid under a perfect zenith illumination and at the starting height). Under these assumptions the optic flow  $\varpi$  seen from the sensor can be computed as

$$\varpi = \frac{v_x}{h} \quad (1)$$

where  $v_x$  represents the ground speed of the spacecraft, and  $h$  is its height above the ground. In Fig. 1b, the output  $\chi$  in volts of the EMD analog circuitry is shown, which is a value that is related to the optic flow  $\varpi$  by a known curve characteristic of the EMD itself. It clearly appears that the EMD is able to detect and measure the asteroid surface irregular shape via the optic flow measurement. At each revolution around the asteroid, while the altitude decreases, the measurements repeat at a higher voltage level, indicating an increase of the optic flow as expected, as the orbital angular velocity is kept constant. Overall, an EMD with a total avionic payload of less than 10 g [14] is able to detect the optic flow at illumination conditions that are typical of a planetary landing. The use of these neuromorphic optic flow sensors during a real spacecraft landing could thus offer a substantial hardware simplification to the primary landing system or a lightweight backup system, adding redundancy to the mission.

Once the optic flow is detected, it is still the guidance algorithm that will have to command the actuators accordingly. Following experiments on bees landing on flat surfaces, Srinivasan et al. [9], Chahl et al. [16], and Thakoor et al. [18] suggest that insects have solved the problem by 1) keeping the optic flow constant throughout their descent and 2) keeping a linear relation between horizontal and vertical speeds. For an EMD-based system, this strategy has the obvious advantage of having key behavioral information (the optic flow) produced directly from the simplest neural unit. The extent to which the Srinivasan et al. [9] hypothesis are actually biologically correct is not discussed here (for a criticism of the second rule of Srinivasan et al., see [20]); instead, some of the possible engineering advantages introduced by such a strategy are discussed. Keeping the optic flow constant during a landing forces the horizontal speed to vanish and the thrust vector to be vertical at touchdown, while it also keeps the visual regime unchanged during the whole descent, allowing fine calibration of all optical instruments and algorithms. The studies by Srinivasan et al. [9], Chahl et al. [16], and Thakoor et al. [18] inspired a number of works dealing with robotic visual navigation. Most of this literature, including the space-related studies [7,8,18], were concerned mainly about the feasibility of a purely neuromorphic approach from the implementation point of view and overlooked the mass optimality of the overall system, which is a key component for a space application. In the following sections, this gap will be filled and a bioinspired guidance algorithm will be proposed that accounts for the peculiarities of a planetary descent where propellant consumption is a design driver.

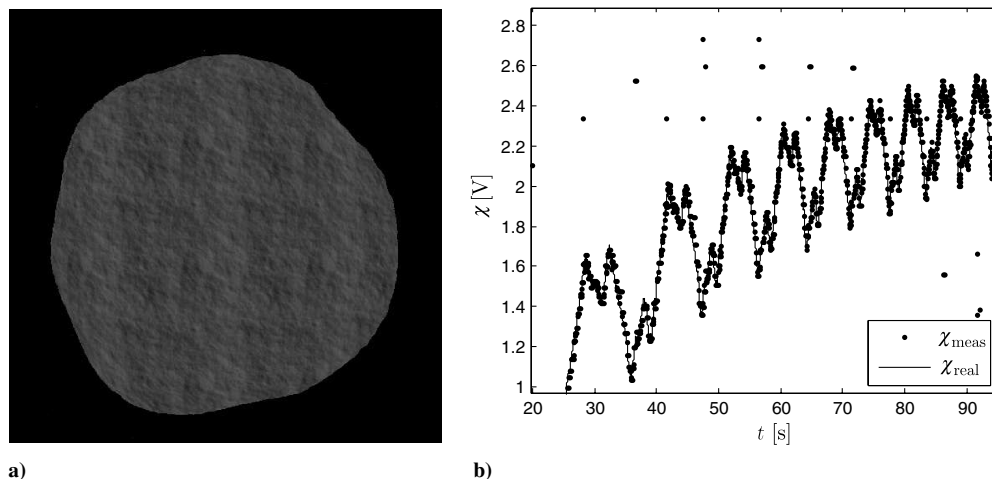


Fig. 1 Simulated readings for an EMD in an asteroid scenario.

### III. Results from the Maximum Principle

In this section constant-optic-flow descents are studied from a theoretical point of view using Pontryagin's maximum principle [21]. The Apollo-like high-gate/low-gate descent that will be used throughout this paper is also introduced as a test case, and its optimal profile is found in this section using a simple shooting method.

#### A. Background

The simplest equations modeling a powered descent of a spacecraft on a planetary surface can be written as

$$\dot{v}_x = \frac{u}{m} \cos \beta \quad (2)$$

$$\dot{v}_z = \frac{u}{m} \sin \beta - g \quad (3)$$

$$\dot{x} = v_x \quad (4)$$

$$\dot{z} = v_z \quad (5)$$

$$\dot{m} = -\frac{u}{I_{sp}g_0} \quad (6)$$

where  $I_{sp}$  is the propulsion system specific impulse. The control variables  $u \in [0, T]$  (where  $T$  is the maximum thrust) and  $\beta$  describe, respectively, the thrust level and the thrust angle. These equations are suited to model only the descent and landing phases of a spacecraft at a preliminary stage, but they are nevertheless very useful to gain insight into the structure of the optimal control. With reference to the equations above, the optimal control problem is studied, minimizing

$$J = \int_0^{t_f} \mathcal{L} dt$$

where  $\mathcal{L}$  is some function of the state and the controls. Following the classical developments from Pontryagin [21], the Hamiltonian function is

$$\mathcal{H} = u \left( \frac{\lambda_{v_x}}{m} \cos \beta + \frac{\lambda_{v_z}}{m} \sin \beta - \lambda_m \frac{1}{I_{sp}g_0} \right) - g\lambda_{v_z} + \lambda_x v_x + \lambda_z v_z + \mathcal{L}$$

where the auxiliary functions  $\lambda$  have the dynamics

$$\dot{\lambda}_{v_x} = -\lambda_x \quad (7)$$

$$\dot{\lambda}_{v_z} = -\lambda_z \quad (8)$$

$$\dot{\lambda}_x = 0 \quad (9)$$

$$\dot{\lambda}_z = 0 \quad (10)$$

$$\dot{\lambda}_m = \frac{u}{m^2} \cos \beta \lambda_{v_x} + \frac{u}{m^2} \sin \beta \lambda_{v_z} \quad (11)$$

Solving the equations above,  $\lambda_x = -b$ ,  $\lambda_{v_x} = a + bt$ ,  $\lambda_z = -d$ , and  $\lambda_{v_z} = c + dt$ . In a time-optimal problem  $\mathcal{L} = 1$ , whereas in a maximum-mass problem  $\mathcal{L} = u$ . In both cases as  $u$  appears linearly in the Hamiltonian, its optimal value in nonsingular arcs will be at the bounds of its admissible region. When  $u = 0$ , i.e., during coast arcs, the equations above all become rather trivial. When  $u = T$ , the mass equation yields

$$m = m_0 - \frac{T}{I_{sp}g_0} t$$

In this case the maximum principle dictates that

$$\tan \beta^* = \frac{\lambda_{v_z}}{\lambda_{v_x}} = \frac{c + dt}{a + bt}$$

which is often referred to as bilinear tangent law. Whenever  $x(t_f)$  is left free (nonpinpoint landing) the transversality condition will dictate  $\lambda_x(t_f) = -b = 0$  and the optimal control will thus follow a linear tangent law (for this textbook example, see also [22]). As a test case, take an Apollo-like scenario [23] and describe the high-gate/low-gate phase of the lunar descent by setting  $T = 45.760$  N,  $I_{sp} = 311$  s,  $m_0 = 9472.06$  kg,  $v_{x_0} = 150$  m/s,  $v_{z_0} = -44$  m/s, and  $h_0 = 2300$  m. As a lunar descent is considered,  $g = 1.623$  m/s<sup>2</sup>. Solving the two-point boundary-value problem resulting from the application of Pontryagin's maximum principle using a single shooting method, the values  $t_f = 44.88$  s and  $m_f = 8798.77$  kg are found in the time-optimal case, and  $t_f = 54.07$  s and  $m_f = 8869.44$  kg are found in the mass-optimal case. The resulting optimal trajectories are visualized in Fig. 2 together with the relation between  $v_x(t)$  and  $z(t)$  during the optimal descent. In the maximum-final-mass case, the descent begins with an unpropelled arc, due to the small value of the chosen high-gate horizontal-speed descents with chosen initial condition  $v_{x_0}$ . It is worth noting that the relation between horizontal speed and height is close to linear in the time-optimal case, and thus the optic flow remains roughly constant during the landing. When a maximum mass is sought, such a relation departs further from linearity, indicating a larger variation of the optic flow. This result comes at no surprise, as insects are far from being mass-varying systems, and thus it would be extremely surprising if they employed landing strategies accounting for mass optimality. Time, on the other hand, is known to insects and is especially important in a phase such as landing, when they are particularly subject to predators.

#### B. Constant Optic Flow

Constant-optic-flow  $\varpi$  descents are studied here considering the relation

$$\varpi z(t) = v_x(t)$$

as a constraint. This constraint can be explicitly accounted for in the equations by considering its differential form:  $\varpi \dot{z} = \dot{v}_x$ . Using Eqs. (2) and (5), an explicit relation between the controls  $\beta$  and  $u$  is found in the form

$$\cos \beta = \frac{m\varpi v_z}{u} \quad (12)$$

which relates the amount of thrust that has to be provided at a certain angle  $\beta$  in order for the optic flow to remain constant during the descent. The degrees of freedom in the control space have thus been reduced by accounting explicitly for the constraint. The equations of motion take the form

$$\dot{v}_z = \pm \sqrt{\frac{u^2}{m^2} - \varpi^2 v_z^2} - g \quad (13)$$

$$\dot{z} = v_z \quad (14)$$

$$\dot{m} = -\frac{u}{I_{sp}g_0} \quad (15)$$

Note the following:

- 1) The control  $u$  now affects the dynamics via a nonlinear term.
- 2) The condition  $T^2/m^2 \geq \varpi^2 v_z^2$  needs to be satisfied at each  $t$  for the system to admit a real solution (remember that  $u \in [0, T]$ ).

Whenever the latter condition is not met, the constant-optic-flow constraint becomes infeasible. The sign in Eq. (13) is also a control variable and determines the quadrant where the thrust lies. Following Pontryagin, [21] the Hamiltonian is

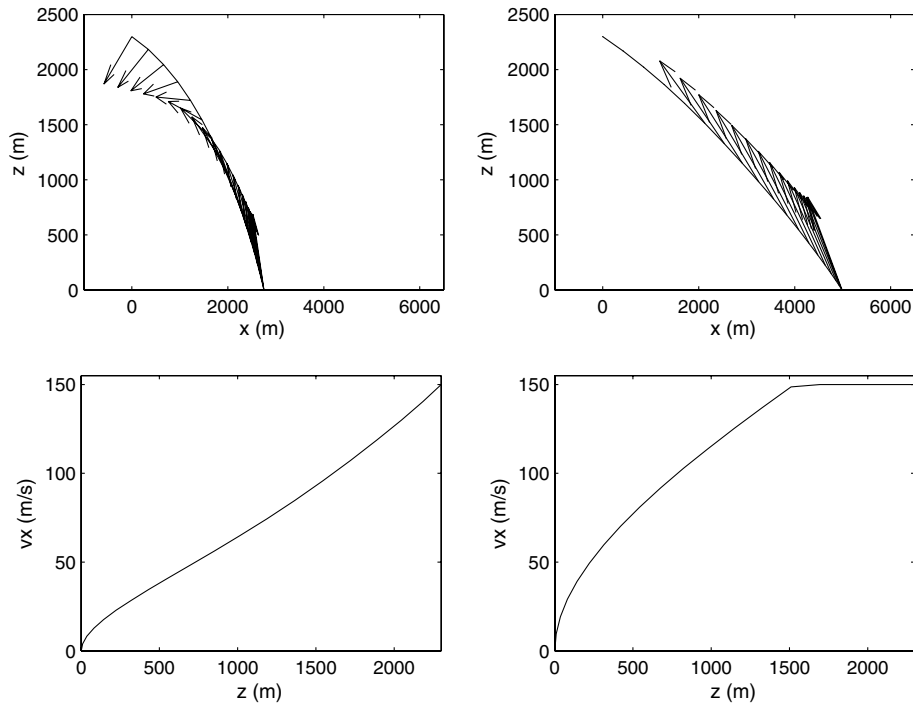


Fig. 2 Time (left) and mass (right) optimal trajectory profiles for the selected high-gate/low-gate test case. Arrows represent the thrust force applied.

$$\mathcal{H} = \lambda_{v_z} \left( \pm \sqrt{\frac{u^2}{m^2} - \varpi^2 v_z^2} - g \right) + \lambda_z v_z - \lambda_m \frac{u}{I_{sp} g_0} + \mathcal{L} \quad (16)$$

$$\cos \beta^* = \frac{(m_0 - \frac{T}{I_{sp} g_0} t) \varpi v_z^*}{T}$$

and derive the dynamics for the auxiliary function:

$$\dot{\lambda}_{v_z} = \pm \lambda_{v_z} \frac{\varpi^2 v_z}{\sqrt{\frac{u^2}{m^2} - \varpi^2 v_z^2}} - \lambda_z \quad (17)$$

$$\dot{\lambda}_z = 0 \quad (18)$$

$$\dot{\lambda}_m = \pm \lambda_{v_z} \frac{u^2}{\sqrt{\frac{u^2}{m^2} - \varpi^2 v_z^2} m^3} \quad (19)$$

Applying the maximum principle to this Hamiltonian, the sign in Eqs. (13), (17), and (19) is decided by the condition  $\pm \lambda_{v_z} \leq 0$ , while the value of  $u$  can be determined analytically by solving the minimization of the Hamiltonian  $\mathcal{H}$ , which is an univariate minimization problem in the form

$$u^* = \arg \min_{u \in [0, T]} -a^2 \sqrt{b^2 u^2 - c^2} - du \quad (20)$$

both for the time-optimal problem ( $\mathcal{L} = 1$ ) and for the maximum-mass problem ( $\mathcal{L} = u$ ). The parameters  $a$ ,  $b$ ,  $c$ , and  $d$  in the expression above descend directly from Eq. (16).

1. Minimum Time

Let us consider in detail the minimum-time optimal control problem to drive a system described by Eqs. (13–15) from a given starting condition  $v_{z_0}, z_0, m_0$  to  $v_{z_f} = 0, z_f = 0$  and free final mass. The transversality condition can be written as  $\lambda_m(t_f) = 0$ . Note that as  $\mathcal{L} = 1$  the coefficient  $d$  in Eq. (20) will always have the sign of  $\lambda_m$ . Given that, in this case,  $\lambda_m$  must be a monotonous decreasing function (see Eq. (19) and that it vanishes at  $t_f$ , then such a sign must always be positive. As a consequence the solution to Eq. (20) is always given by  $u^* = T$  and the optimal thrust angle is

Thus, along time-optimal descents with free ending point and constant optic flow,

$$\dot{v}_z^* = \pm \sqrt{\frac{T^2}{(m_0 - \frac{T}{I_{sp} g_0} t)^2} - \varpi^2 v_z^{*2} - g}$$

The sign in the equation above has to be taken as negative for  $t \in [0, t_{sw})$  and positive for  $t \in (t_{sw}, t_f]$ , where  $t_{sw}$  represents the switching time when  $\lambda_{v_z} = 0$  and  $t_f$  the time when the condition  $v_z(t_f) = 0$  is satisfied. The switching time can then be found efficiently via a simple iterative procedure to solve the equation  $z(t_f) = 0$  letting  $t_{sw}$  vary while keeping  $v_z(t_{sw}) < 0$ . The cases where the initial sign of the equation is positive are those in which  $z(t_{sw}) < 0$ , and they are infeasible, as they correspond to trajectories crashing on the ground. Considering the case study of the Apollo-like descent presented in the previous section the optimal solution visualized in

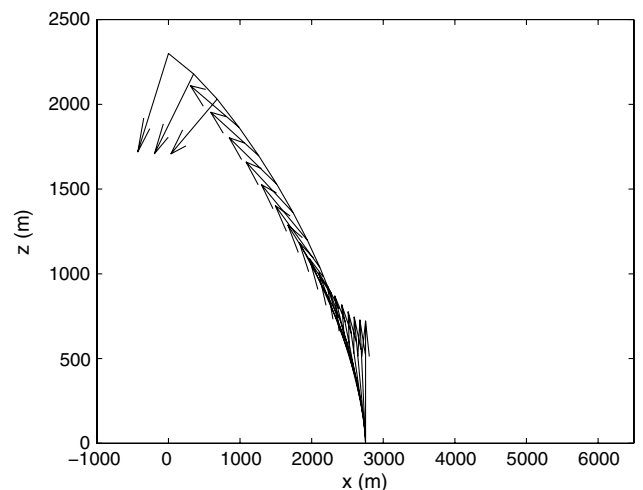
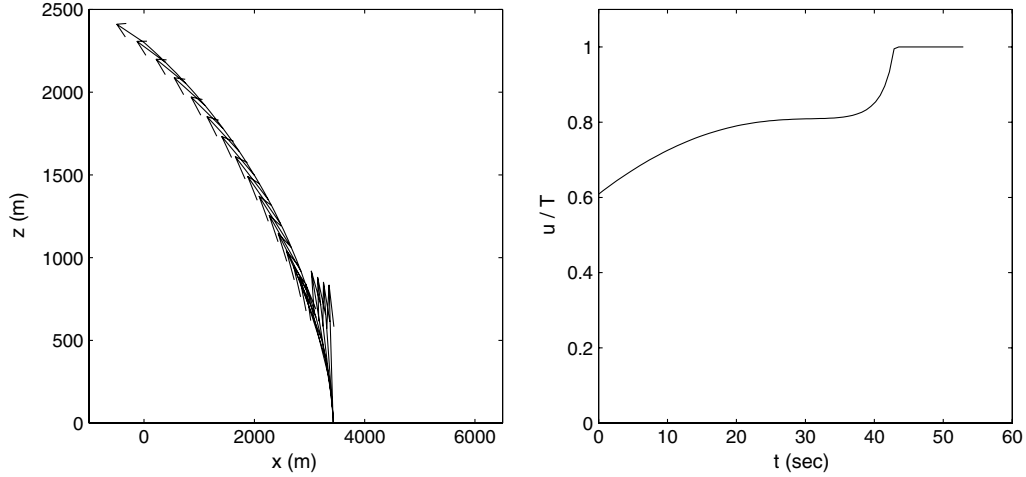


Fig. 3 Time-optimal descent in our case study. Optic flow is kept constant throughout the trajectory.



**Fig. 4** Mass-optimal descent in our case study. Optic flow is kept constant throughout the trajectory. The optimal value for  $u^*$  is not always in the border of its allowed region.

Fig. 3 achieves the final landing in  $t_f = 45.54$  s and with a final mass  $m_f = 8789.01$  kg. The pitch angle  $\beta$ , because of the dynamical model used, switches between values, making the thrust vectoring more challenging from an engineering point of view. A refined dynamical model including attitude control will be used later and will produce smooth pitch profiles in all cases.

## 2. Maximum Mass

Now consider the case  $\mathcal{L} = u$ , corresponding to the maximization of the final lander mass. The only difference with respect to the previous case is in Eq. (20), where now  $d = 1 - \lambda_m(T/I_{sp}g_0)$ . The application of Pontryagin's maximum principle to this case is more difficult, as no general conclusion can be made on the solution of Eq. (20), which will thus need to be considered on a case-by-case basis. Using a simple single shooting method to solve the resulting two-point boundary-value problem in the test case introduced, the solution shown in Fig. 4 achieves the landing in  $t_f = 52.91$  s and with a final mass  $m_f = 8824.74$  kg. The single shooting method has quite some difficulties in finding the solution to the two-point boundary-value problem as the radicals in the system of equations often become undefined during a shooting and at the final point where  $z_f = 0$  and thus the optic flow definition becomes undetermined. This makes the radius of convergence of the method even smaller than usual. The solution presented here was found after many multistarts randomly initialized the initial costates and tricked the search algorithm with heuristics, driving the search away from infeasible zones.

## C. Discussion

The application of Pontryagin's maximum principle to a simple planetary descent model shows that the optimal pitch law is affected by constraining the optic flow to be constant during the descent. In particular, the linear tangent law is no longer optimal for the latter case and is replaced by a more complex law. In the case of the time-optimal constant-optic-flow trajectory it is demonstrated that the value of the optimal control is constantly saturated to  $u^* = T$  as in the unconstrained case, while the optimal pitch law changes according to Eq. (12). The maximum-mass case is more complex and the effect of the added constraint modifies the optimal control structure entirely, allowing for  $u^*$  to assume values other than one. In Table 1 a summary of the conclusions drawn in the previous sections is shown, reporting the functional expressions obtained for the optimal pitch law and the numerical values of the final mass  $m_f$  and  $t_f$  found solving the optimal control problem for the test case selected, modeling an Apollo-like high-gate/low-gate descent. While time-optimal trajectories do not change much when adding the constant-optic-flow constraint, mass-optimal trajectories do, and it is thus critical to study these cases more in depth to assess the feasibility of using constant-optic-flow descents during planetary landings.

## IV. Direct Approach

To extend the numerical results obtained in the previous sections allowing a thorough numerical experimentation on more complex dynamics, different objective functions, different boundary conditions and path constraints, a direct approach based on the impulsive transcription of the control history is implemented. The algorithm has been developed for this particular study and is available as open-source project named spaceAMPL in the SourceForge repositories. The algorithm was developed with the aim to avoid convergence problems, initial guess selection problems and to return a solution in short CPU times to allow extensive Monte Carlo experimentations. Existing popular direct approaches (e.g., based on Hermite-Simpson or pseudo spectral collocation methods) could also have been used for the purpose of the calculations reported here, but our expertise on optimal control developed in the field of interplanetary trajectory optimization lead us to a different choice.

### A. Impulsive Method

In 1999, Sims and Flanagan [24] presented a direct optimization method intended to be used for the design of low-thrust interplanetary trajectories. A number of papers [25–29] have been devoted to show the merits of this method for the design and optimization of low-thrust, gravity-assist trajectories. The original motivation for the development of such a method was rooted into being able to perform a preliminary mission design willing to accept reduced accuracy to achieve a robust algorithm. In the first part of this section a general method to solve optimal control problems, inspired by the original Sims and Flanagan's paper, is introduced and its accuracy is studied for the case of finding optimal planetary descents. Consider the following optimal control problem (i.e., a Mayer problem with inequality path constraints and linear dynamics in the controls):

$$\begin{cases} \min_{\mathbf{u} \in \mathcal{U}} J = \Phi(\mathbf{x}(t_0), t_0, \mathbf{x}(t_f), t_f) \\ \dot{\mathbf{x}} = \mathbf{f}(\mathbf{x}) + \mathbf{B}\mathbf{u} \\ \mathbf{b}(\mathbf{x}(t_0), t_0, \mathbf{x}(t_f), t_f) = 0 \\ \mathbf{p}(\mathbf{x}(t), t) \leq 0 \end{cases} \quad (21)$$

**Table 1** Summary of the optimal pitch laws

Case	Optimal pitch law	$m_f$ , kg	$t_f$ , s
Minimum time	$\tan \beta^* = a + bt$	8798.77	44.88
Maximum mass	$\tan \beta^* = a + bt$	8869.44	54.07
Minimum time (OF = const)	$\cos \beta^* = m\varpi v_z^*/T$	8789.01	45.54
Maximum mass (OF = const)	$\cos \beta^* = m\varpi v_z^*/u^*$	8824.74	52.91

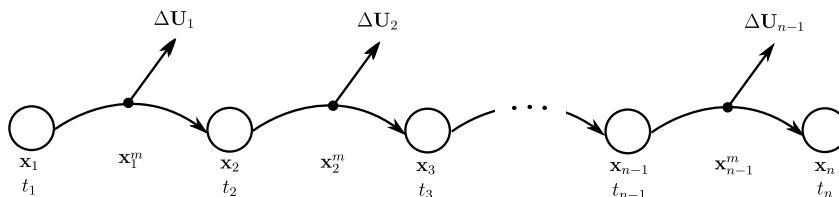


Fig. 5 Discretization of the state and control variables for the impulsive model.

and introduce a mesh  $t_0 = t_1 > t_2 > \dots > t_n = t_f$  of  $n$  points on the time interval  $[t_0, t_f]$ . Assume the control  $\mathbf{u}$  has the following functional form:

$$\mathbf{u}(t) = \sum_{i=1}^{n-1} \Delta \mathbf{U}_i \delta(t - t_i^m) \quad (22)$$

where  $\delta(t - t_i^m)$  is the Dirac delta function and  $t_i^m = (t_{i+1} + t_i)/2$  are the time instants falling in the middle of each mesh segment. Introduce the impulse magnitude  $\Delta U_i$  and constrain it by setting

$$\min_{\mathbf{u} \in \mathcal{U}} \left( \int_{t_i}^{t_{i+1}} |\mathbf{u}| dt \right) \leq \Delta U_i \leq \max_{\mathbf{u} \in \mathcal{U}} \left( \int_{t_i}^{t_{i+1}} |\mathbf{u}| dt \right)$$

thus making sure that the approximated control does not provide impulses conflicting with the original definition of the functional space  $\mathcal{U}$ .

See Fig. 5 for a visualization of the discretization of the time line and of the nomenclature used to indicate the state and the time in the grid points and on the midpoints, in particular,  $\mathbf{x}_1, \mathbf{x}_2, \dots, \mathbf{x}_n$  are the states in the nodes,  $t_1, t_2, \dots, t_n$  the times,  $\mathbf{x}_1^m, \mathbf{x}_2^m, \dots, \mathbf{x}_{n-1}^m$  are the state in the midpoints of a segment, and  $\Delta \mathbf{x}_1, \Delta \mathbf{x}_2, \dots, \Delta \mathbf{x}_{n-1}$  represent the discontinuities caused by the impulses  $\Delta \mathbf{U}_1, \Delta \mathbf{U}_2, \dots, \Delta \mathbf{U}_{n-1}$ . Trivially, from the linearity in the controls of the system dynamics, these discontinuities can be evaluated as  $\Delta \mathbf{x}_i = \mathbf{B} \cdot \Delta \mathbf{U}_i$  (in the case of a system that is not linear in the controls these discontinuities have a more complex expression representing the impulsive response). Using this discretization the dynamics in the nodes  $\mathbf{x}_i$  can be evaluated as a function of the impulse magnitudes recursively applying the equation

$$\mathbf{x}_{i+1} = \phi(\phi(\mathbf{x}_i, t_i, t_i^m) + \Delta \mathbf{x}_i, t_i^m, t_{i+1}) \quad (23)$$

where  $\phi(\mathbf{x}, t_1, t_2)$  represents the propagation up to  $t_2$  of the unperturbed dynamics  $\dot{\mathbf{x}} = \mathbf{f}(\mathbf{x})$  starting from  $\mathbf{x}$  at  $t_1$ . Such a propagation represents the evolution of the uncontrolled system and often admits an analytical solution, making the resulting computer implementation fast and efficient. Consider the nonlinear programming problem (NLP) associated with the optimal control problem stated in Eq. (21):

Find

$$t_1, t_n, \Delta U_i \quad i = 1, \dots, n-1$$

To minimize

$$J = \Phi(\mathbf{x}_1, t_1, \mathbf{x}_n, t_n) \quad (24)$$

Subject to

$$\mathbf{b}(\mathbf{x}_1, t_1, \mathbf{x}_n, t_n) = 0$$

$$p_i(\mathbf{x}_i, t_i) \leq 0 \quad i = 1, \dots, n$$

$$\Delta U_i \leq (t_{i+1} - t_i) \bar{u} \quad i = 1, \dots, n-1$$

where it is assumed, for simplicity, that the functional space  $\mathcal{U}$  contains all piecewise continuous functions  $\mathbf{u}$  such that  $0 \leq |\mathbf{u}| \leq \bar{u}$ . In the above system the  $\mathbf{x}_i$  are a function of the NLP problem variables via Eq. (23) substituting to  $\Delta \mathbf{x}_i$  their functional dependence in terms of the  $\Delta U_i$ . All times  $t_i$  are assumed to be dependent on  $t_1$

and  $t_n$ . In this implementation an equally spaced mesh is considered so that  $t_i = t_1 + (t_n - t_1)/(n-1)(i-1)$ .

## B. Accuracy

To test the accuracy and speed of the numerical approach devised in the previous section, consider the test case introduced previously, apply the impulsive transcription method, vary the number of nodes, and compare the results with those reported in Table 1. To apply the formal developments of the previous section, note that Eqs. (2–6) are not in the simple form  $\dot{\mathbf{x}} = \mathbf{f}(\mathbf{x}) + \mathbf{B}\mathbf{u}$ . Thus, consider  $u_z = u \sin \beta$  and  $u_x = u \cos \beta$  as controls and calculate the discontinuities caused by the impulsive controls using the equations of motion as

$$\Delta m = -\sqrt{\Delta U_x^2 + \Delta U_z^2} / I_{sp} g_0, \quad \Delta v_x = \Delta U_x / (m + \Delta m / 2)$$

$$\Delta v_z = \Delta U_z / (m + \Delta m / 2)$$

To define the resulting NLP problem, the modeling language for mathematical programming (AMPL), popular within the operation research community, is used here. The great advantage of using such a tool stems from the possibility of formalizing optimization problems in a metaprogramming language closer to humans than to computers. The problem description is uncoupled to the particular solver used, and its interface to the solver is provided automatically by AMPL, together with all the derivatives. The AMPL models developed and used here are made available via SourceForge under the open-source general public license as part of the spaceAMPL project of the Advanced Concepts Team. The results obtained using the sequential-quadratic-programming-based solver SNOPT are shown here, as this solver is quite common in the aerospace community. The results can be reobtained by submitting the AMPL models available through spaceAMPL to the near-Earth-object online free service.<sup>§</sup> Constant-optic-flow descents are simply obtained, adding the path constraints  $p_i(\mathbf{x}_i, t_i) = \varpi z_i - v_{xi} = 0$  ( $i = 1, \dots, n$ ) to the problem description. The initial guess used for all simulations is the free-fall trajectory resulting from the initial conditions. In Fig. 6 the case of the minimum time descent is reported, and results for the maximum mass are reported in Fig. 7. The absolute errors reported in the figures refer to the difference with the solution obtained previously using Pontryagin's theory and reported in Table 1. The data reported are relative to Intel Xeon X5355 CPUs. This brief experimental study shows that the impulsive method is also an efficient direct optimization technique for systems that are different from the interplanetary trajectory for which it was originally devised. Already using a small number of nodes (resulting in fast CPU times), it provides good approximations for the optimal value of the objective function and for the optimal descent trajectory.

## V. Increasing the Complexity

A more complex representation of the descent dynamic is introduced here and will be used in the rest of this work. As observed, a limitation of the model described by Eqs. (2–6) is the absence of the spacecraft attitude dynamics. Optimal solutions to these equations can be used as a command to an outer control layer tasked to make sure to actuate the spacecraft attitude to thrust as close as possible to the optimal direction during the whole descent. The lander attitude is now accounted for directly in the equations. Consider the following dynamics,

<sup>§</sup>Data available online at <http://neos.mcs.anl.gov/neos/>.

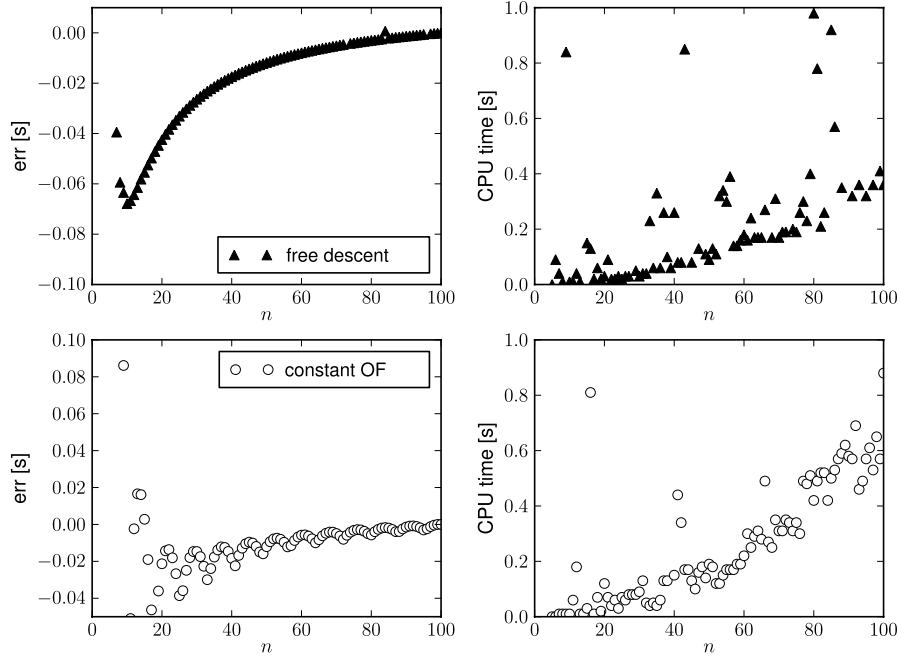


Fig. 6 Performance of the direct impulsive optimization method for the minimum-final-time case.

$$\dot{x} = v_x \quad (25)$$

$$\dot{v}_x = \frac{u_1 + u_2 + u_3}{m} \cdot \cos \beta \quad (26)$$

$$\dot{z} = v_z \quad (27)$$

$$\dot{v}_z = \frac{u_1 + u_2 + u_3}{m} \cdot \sin \beta - g \quad (28)$$

$$\dot{\beta} = \omega \quad (29)$$

$$\dot{\omega} = (u_2 - u_3) \frac{R}{I} \quad (30)$$

$$\dot{m} = -\frac{u_1 + u_2 + u_3}{I_{sp} \cdot g_0} \quad (31)$$

which describe the descent of a spacecraft equipped with a main engine delivering the thrust  $0 \leq u_1 \leq T_1$  and two lateral engines tasked to control the spacecraft pitch angle  $\beta$  and its angular velocity  $\omega$  delivering a thrust  $0 \leq u_2 \leq T_2$  and  $0 \leq u_3 \leq T_2$  at an offset  $\pm R$  from the spacecraft center of mass, where  $I$  is the spacecraft rotational inertia. Also for this system, the uncontrolled dynamics [and thus the function  $\phi(\mathbf{x}, t_1, t_2)$  in Eq. (23)] admit a simple analytical solution. To simplify the description of the control space and reduce the number of variables in the resulting NLP, the following control variables are used:  $\tilde{u}_1 = u_1 + u_2 + u_3$  and  $\tilde{u}_2 = u_2 - u_3$  (directly related to the total thrust and the total torque). The description of the control space  $\mathcal{U}$  becomes  $|\tilde{u}_2| \leq \tilde{u}_1 \leq T_1 + 2T_2 - |\tilde{u}_2|$  and  $-T_2 \leq \tilde{u}_2 \leq T_2$ , while the functional relation between  $\Delta \mathbf{x}$

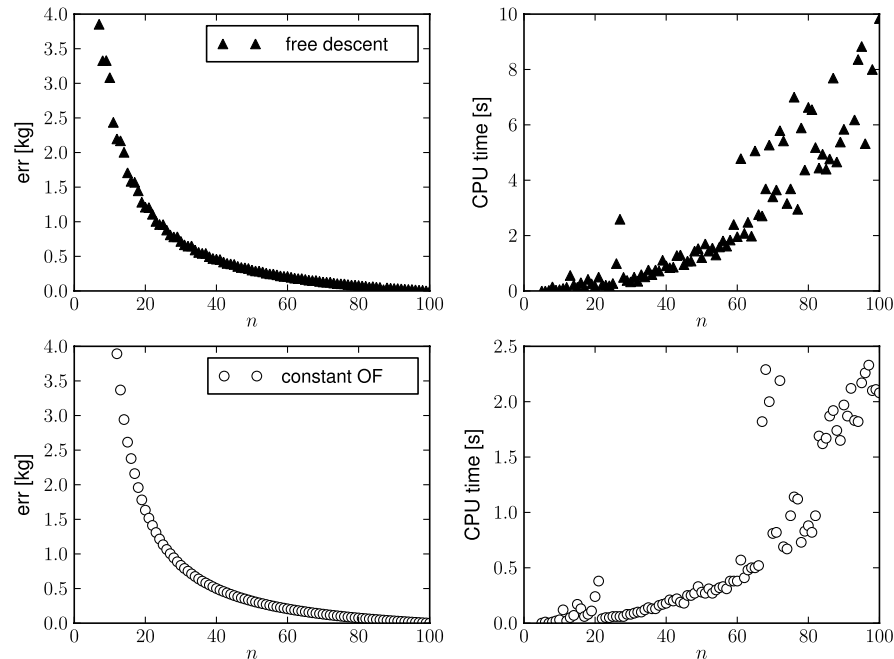


Fig. 7 Performance of the direct impulsive optimization method for the maximum-final-mass case.

and  $\Delta U$  that is necessary to write the impulsive transcription of the maximum final mass optimal control problem can be written as

$$\Delta m = -\Delta \tilde{U}_1 / I_{sp} g_0, \quad \Delta \beta = \Delta \tilde{U}_2 R / (I + \Delta I / 2)$$

$$\Delta v_x = \Delta \tilde{U}_1 \cos(\beta + \Delta \beta / 2) / (m + \Delta m / 2)$$

$$\Delta v_z = \Delta \tilde{U}_1 \sin(\beta + \Delta \beta / 2) / (m + \Delta m / 2)$$

The resulting NLP can be formalized using AMPL and is also made available via the SourceForge project spaceAMPL. The model is used to study the mass optimality of constant-optic-flow descents with various high-gate conditions during an Apollo-like spacecraft.

Note that the pitch dynamics during a planetary landing can be quite rich, with pitch angles that vary of large amounts. This has a nonnegligible effect on the reading of the EMD sensor. One option to face this issue is to envisage the EMD as gimballed with a passive mechanism, allowing it to always point downward. Another option is to leave the EMD fixed in the body frame and use an estimate of the spacecraft angular velocity  $\omega$  and of its pitch angle  $\beta$  to correct for the sensor reading. In this second case, and approximating the optical paths of each photodetector as equal, the geometrical relation  $\varpi = (v_x/h) \sin \beta + \omega$  relates the optic flow to the spacecraft state and has to be used instead of Eq. (1). Both of these options need further assessment details to fully understand their implication on the landing system performance and design. In the rest of this paper a perfectly-nadir-pointing EMD will be assumed when relating the optic flow to the spacecraft state [i.e., Eq. (1) is used].

#### A. Could Apollo Land Using a Constant-Optic-Flow Descent?

Consider the typical Apollo-like three-phase profile for a lunar descent (Fig. 8). During the first phase, the spacecraft orbiting the planet starts from high speeds (1.7 km/s) at an altitude of roughly 15 km and slows down to speeds of the order of 100 m/s while decreasing its height to 2.3 km, reaching what are commonly referred to as high-gate conditions. The second phase (which will be studied

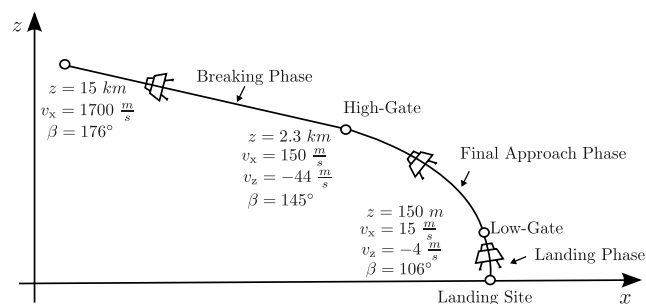


Fig. 8 Three descent phases for an Apollo lunar landing scenario with typical values for high gate and low gate taken from [23].

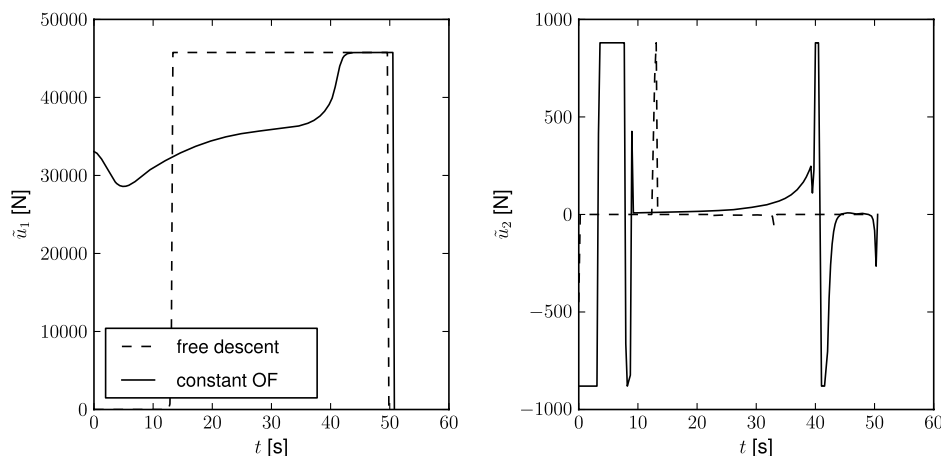


Fig. 9 Controls during an optimal high-gate/low-gate descent: solid line refers to a constant-optic-flow descent.

Table 2 Boundary conditions at high gate (equality) and low gate (inequality)

	$x, m$	$v_x, m/s$	$z, m$	$v_z, m/s$	$\beta, ^\circ$	$\omega, deg/s$	$m, kg$
High gate	0	150	2300	-44	145	0	9472
Low gate	Any	15	150	-4	Any	Any	Max

here in more detail to assess the impact of keeping the optic flow constant during the descent) brings the spacecraft from high-gate to low-gate conditions, characterized by a height of 150 m and a speed of 15 m/s. The last phase actually accomplishes the planetary landing, bringing the spacecraft from low gate to touchdown.

The second phase of the descent is considered here, and the optimal-final-mass descent is computed using the boundary conditions reported in Table 2, with and without forcing a constant optic flow throughout the descent. For the spacecraft rotational inertia the simple assumption  $I = 1/2 m R^2$  is made, with  $R = 3 m$ . Also consider  $T_1 = 44,000 N$  and  $T_2 = 880 N$ . The resulting optimal control profiles are reported in Fig. 9, and the spacecraft state during the optimal descent is reported in Fig. 10. Note that the impulsive transcription method copes well with the added complexity in the dynamics and is able to calculate the optimal descent profile while optimizing the attitude dynamics. Forcing a constant optic flow throughout the trajectory increases the complexity in the rotational dynamics (and thus control history), as the spacecraft still needs to satisfy Eq. (12) at each time instant in order to keep the optic flow constant.

Let us vary the high-gate starting conditions and calculate the resulting variation of the optimal final mass. In particular, vary the values for the starting height  $z_0$ , the starting horizontal velocity  $v_{x_0}$ , and the starting vertical velocity  $v_{z_0}$ . The ranges used for each one of these variables are reported in Table 3 together with the resulting maximum, minimum, and average values of the propellant mass penalty  $\Delta P$  introduced by the constant-optic-flow strategy. This is defined as the relative difference between the propellant mass used during an optimal constant-optic-flow descent and a free optimal descent. The number of nodes used to run the impulsive method was  $n = 40$ .

In Fig. 11 the final optimal masses are plotted against the starting high-gate conditions. Note that the variation is quite mild and linear, both for the constant-optic-flow descent and for the free-descent cases. As a rule of thumb, the cost of forcing a constant optic flow during a lunar high-gate/low-gate descent of an Apollo-like capsule can be estimated to be around 10% of propellant and an added complexity of the thrust history. Thus, there would be little reason to consider a constant-optic-flow descent as a baseline for a lunar landing, as far as the potential hardware and software simplifications introduced by the neuromorphic approach are proven to be actually worth the 10%, while it seems reasonable to assume that constant-optic-flow descents can be considered as a backup option to activate

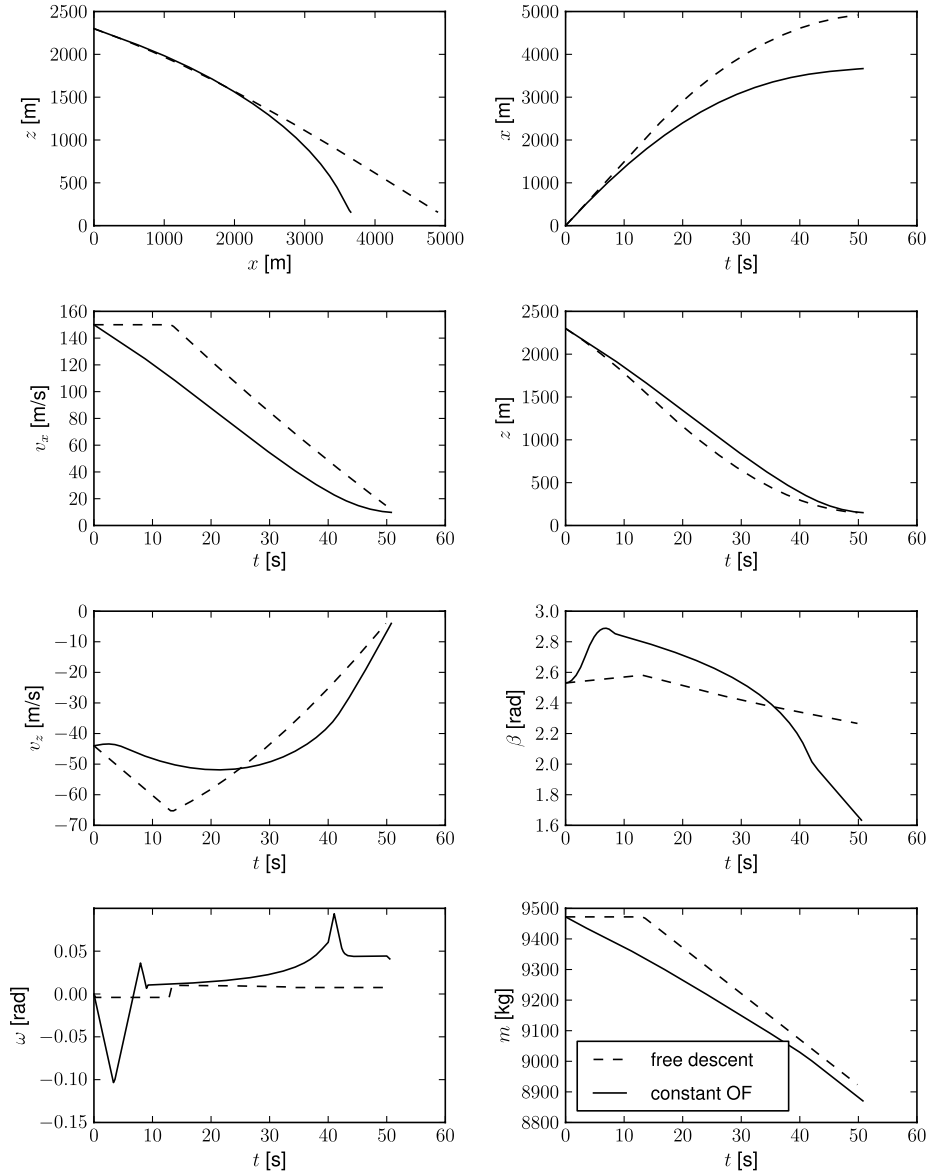


Fig. 10 State variables during an optimal high-gate/low-gate descent: solid line refers to a constant-optic-flow descent.

in case an emergency landing is needed. In this case, the interest in the neuromorphic solution derives from its inherent robustness and adaptiveness, which are necessary properties of emergency actions. The calculations presented here were made under a number of assumptions made on the lander design. The real mass penalty introduced by the constant-optic-flow descent would need to be reevaluated on a case-to-case basis, as it does depend on the thruster technology used and their configuration. It is nevertheless interesting to have obtained an order-of-magnitude estimate in a realistic case.

### B. Importance of Being Tuned (Choosing the Correct Pitch)

In [8] the authors propose a neuromorphic approach for a lunar landing scenario. The autopilot described there directly derives from the EMD-based OCTAVE-autopilot principles developed in the context of Earth applications [14]. This employs two-dimensional spacecraft dynamics, similar to those used in this paper, but assumes the pitch law (thrust angle) to have some functional form known in advance. Three cases for the commanded pitch law  $\beta(t)$  are discussed in [8]:

$$\beta(t) = \begin{cases} c_1 c_2^{t/\tau} \\ c_3 + c_4 t \\ \beta_0 \end{cases} \quad (32)$$

where  $c_1 = \beta_0$ ,  $c_2 \in (0, 1)$ ;  $\tau = 15, 20$ , and  $25$  s;  $c_3 = \beta_0$ ; and  $c_4 = 1, 0.5, 0.25$ , and  $0.125$  deg/s.

The authors compare the different scenarios with respect to the landing duration, the velocities at low gate, and the fuel consumption. The best results are reported for a linear pitch law with a slope of  $0.25$  and  $0.125$  deg/s, with a propellant consumption of  $176$  kg, and  $170.9$  kg, respectively [8].

Now consider the same simple dynamics of Eqs. (2–6) and add one degree of freedom relative to the pitch angle, assuming to control it directly:

$$\dot{x} = v_x \quad (33)$$

$$\dot{v}_x = \frac{u_1}{m} \cdot \sin \beta \quad (34)$$

Table 3 Relative final propellant mass difference between optimal and constant-optic-flow strategies by variation of  $v_{x_0}$ ,  $v_{z_0}$ , and  $z_0$

Parameter	Range	$\Delta P_{\max}$	$\Delta P_{\text{mean}}$	$\Delta P_{\min}$
$v_{x_0}$ , m/s	170 to 120	11.39%	8.66%	6.71%
$v_{z_0}$ , m/s	-22 to -65	9.65%	8.53%	7.13%
$z_0$ , m	3300 to 2300	11.66%	10.02%	8.49%

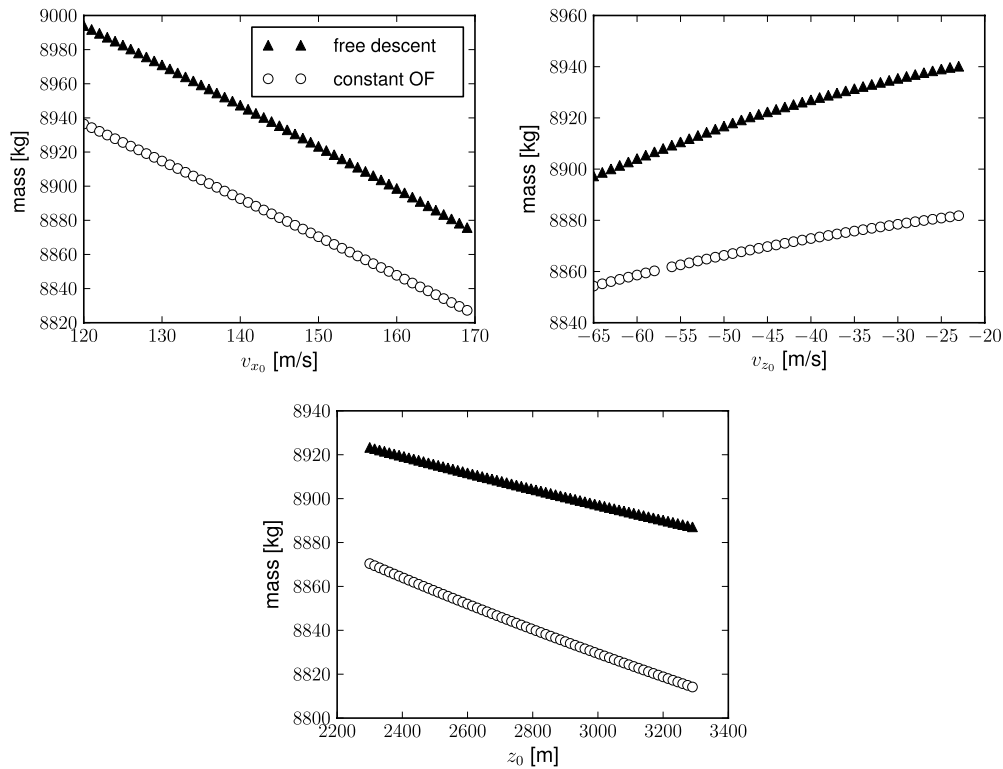


Fig. 11 Optimal final mass, varying the high-gate conditions.

$$\dot{z} = v_z \quad (35)$$

$$\dot{v}_z = \frac{u_1}{m} \cdot \cos \beta - g \quad (36)$$

$$\dot{\beta} = u_2 \quad (37)$$

$$\dot{m} = -\frac{u_1}{I_{sp} \cdot g_0} \quad (38)$$

Consider the high-gate/low-gate descent optimal control problem relative to the dynamics presented above and use the values used in [8] to define the spacecraft design and the boundary conditions (i.e., the constraints on the initial and final spacecraft states). Note that now, at the end of the descent, the spacecraft is brought to 150 m altitude from touchdown.

Three different optimal control problems to maximize the final spacecraft mass can be considered for the purpose of a comparison with the results reported in [8]: 1) leaving the pitch free to vary optimally, 2) constraining the maximum value of the pitch rate  $u_2$  to the maximum value of the exponential, and 3) constraining the maximum value of the pitch rate  $u_2$  to the maximum value of the linear pitch laws used in [8]. The implementation of the different dynamics and constraints is straightforward using an impulsive transcription to solve these optimal control problems. The resulting AMPL model is also made available in the open-source spaceAMPL SourceForge project.

A summary of the results found is shown in Table 4, and Fig. 12 reports the different pitch laws mentioned. Clearly, the employment of optimal pitch laws is essential to the efficiency of the resulting descent profile, as it results in the use of one-fourth of the propellant mass and in a shorter descent time. In conclusion, the neuromorphic autopilot proposed and implemented in [8] for a lunar descent can be significantly further improved by developing methods to generate near-optimal pitch laws.

## VI. Constant-Optic-Flow Descent Guidance Scheme

The solutions found in previous sections are based on optimal control theory and related numerical techniques. These are typically computationally too expensive to be used in a real-time onboard guidance loop. Computationally inexpensive approaches can be developed that, though not optimal, try to make efficient use of the available resources. A simple guidance scheme is thus proposed and compared with the optimal constant-optic-flow descents. Aiming at a fully bioinspired approach, one could take the two landing principles observed by Chahl et al. [16] in bees and then engineer a guidance algorithm that 1) keeps the optic flow constant and 2) keeps a linear relation between vertical and horizontal speeds. The validity of the second point can be verified along an optimal spacecraft descent trajectory (be it with or without the constant optic flow forced to be constant) by plotting the relevant quantities as shown in Fig. 13 for one of the optimal trajectories computed numerically for an Apollo-like lunar descent. From these plots, it seems that the relation between  $v_x$  and  $v_z$  is far from being linear during a mass-optimal descent, especially if a constant optic flow is forced. Exploiting this insight and noting, on the other hand, that the relation between time

Table 4 Comparison of the descents employing the different pitch laws

Pitch Law	Optimal	Experiment <sup>a</sup>	Optimal (experiment)	Linear <sup>a</sup>	Optimal (linear)
Landing duration, s	18.61	55.2	47.11	63.3	37.02
Propellant, kg	53.75	201.4	62.48	210	58.59
Landing distance, m	1096.15	2660	1967.61	2700	1647.12

<sup>a</sup>Taken from [8].

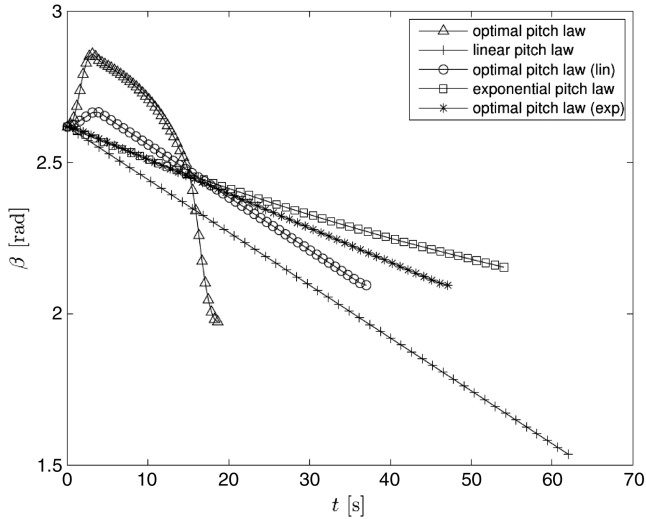


Fig. 12 Different pitch laws used in the comparison.

and  $v_x$  is more easily approximated, a full bioinspiration is abandoned here, and a guidance algorithm is proposed that keeps the optic flow constant to take advantage of the inherent robustness of such a strategy, but that also aims to keep a polynomial relation between time and horizontal velocity. The resulting scheme takes inspiration from the original Apollo's guidance algorithm [10] and modifies it in order to include the constant-optic-flow regulation. The approach followed here refers to the simple model in Eqs. (2–6).

Let us start from the following form for the horizontal acceleration:

$$\dot{v}_x = a_{x_{cmd}} = \varpi v_{z_0} + \sum_{i=1}^N c_i t^i$$

where the coefficients  $c_i$  entirely define its shape. Adopting such an expression for the horizontal acceleration and forcing a constant ventral optic flow from Eq. (1), we have

$$v_z = v_{z_0} + \sum_{i=1}^N \frac{c_i}{\varpi} t^i$$

Now target particular values for the descent total duration, for the final vertical velocity, for the final horizontal velocity, and for the final range ( $t_f, v_{z_f}, v_{x_f}, x_f$ ). Limit the polynomial expansion to the third degree and find unique values for the coefficients  $c_i$  by writing the explicit form of the target values:

$$\left. \begin{aligned} c_1 t_f + c_2 t_f^2 + c_3 t_f^3 &= \varpi(v_{z_f} - v_{z_0}) \\ c_1 \frac{t_f^2}{2} + c_2 \frac{t_f^3}{3} + c_3 \frac{t_f^4}{4} &= (v_{x_f} - v_{x_0}) - \varpi v_{z_0} t_f \\ c_1 \frac{t_f^3}{6} + c_2 \frac{t_f^4}{12} + c_3 \frac{t_f^5}{20} &= (x_f - x_0) - v_{x_0} t_f - \frac{\varpi v_{z_0}}{2} t_f^2 \end{aligned} \right\} \rightarrow \mathbf{A} \mathbf{c} = \mathbf{b}$$

which is a linear system in the unknown coefficients  $c_i$ . Inverting such a system, the various  $c_i$  are found as a function of the targeted values  $t_f, v_{z_f}, v_{x_f}$ , and  $x_f$ , and thus the whole targeted descent profile is determined. The inverse of matrix  $\mathbf{A}$  has the form

$$\mathbf{A}^{-1} = \begin{bmatrix} 3/t_f & -24/t_f^2 & 60/t_f^3 \\ -12/t_f^2 & 84/t_f^3 & -180/t_f^4 \\ 10/t_f^3 & -60/t_f^4 & 120/t_f^5 \end{bmatrix}$$

The relationships with respect to the required thrust and pitch angle to be actuated during such a descent can be easily found by inverting Eqs. (2) and (3):

$$u^2 = m^2[\dot{v}_x^2 + (\dot{v}_z + g)^2] \quad \tan \beta = \frac{\dot{v}_z + g}{\dot{v}_x}$$

In Fig. 14 the resulting descent trajectory is shown together with the required throttle  $u$  magnitude in the same lunar descent case used previously. A perfect soft landing is targeted; thus,  $v_{z_f} = v_{x_f} = 0$  (the condition  $z_f = 0$  is automatically ensured by the constant-optic-flow constraint). The descent duration and the horizontal range are the only values left for guessing. For this example the values  $x_f = 3346$  m and  $t_f = 52.91$  s are used. The target time is taken from its optimal value, while the range is evaluated analytically to make  $u = T$  at touchdown. The resulting descent is compared with the optimal (see Fig. 4), observing a good accordance. In this case the final mass of the spacecraft at touchdown is 8822.12 kg, against the 8824.74 kg of the optimal value. The guidance scheme proposed can thus approximate the optimal constant-optic-flow descent satisfactorily.

Our approach is similar to the original Apollo's guidance scheme, as reported in previous work [10]. The main difference here is that a constant optic flow is forced during the descent. By specifying  $\dot{v}_x$  together with optic flow constraint, the entire trajectory is determined from boundary conditions, allowing fast and efficient onboard calculations that generate reference descent profiles that are close to optimal constant-optic-flow descents. Our guidance law, thanks to the inherent properties of the constant-optic-flow strategy, always guides toward a soft landing (also in the presence of disturbances or faults) as long as the horizontal acceleration keeps being decreased and the optic flow is kept constant. The timely update of the target quantities, and thus of the coefficients from the guidance loop, is thus not as crucial to the landing success, only to its optimality.

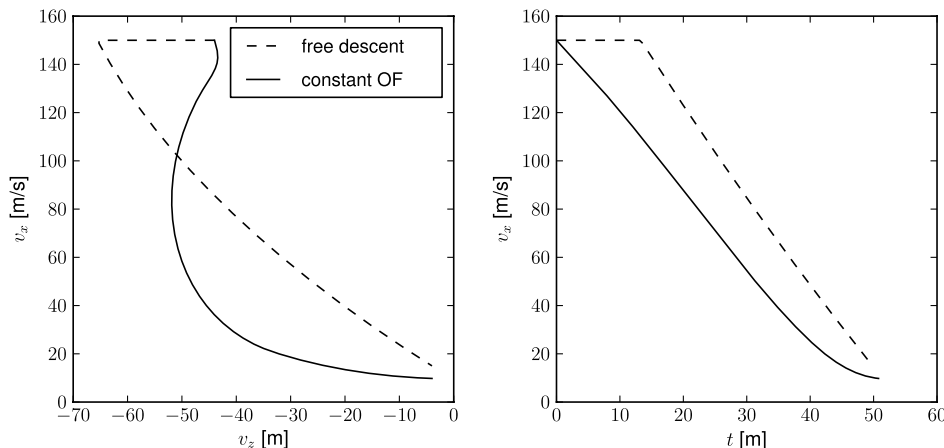


Fig. 13 Linear relations.

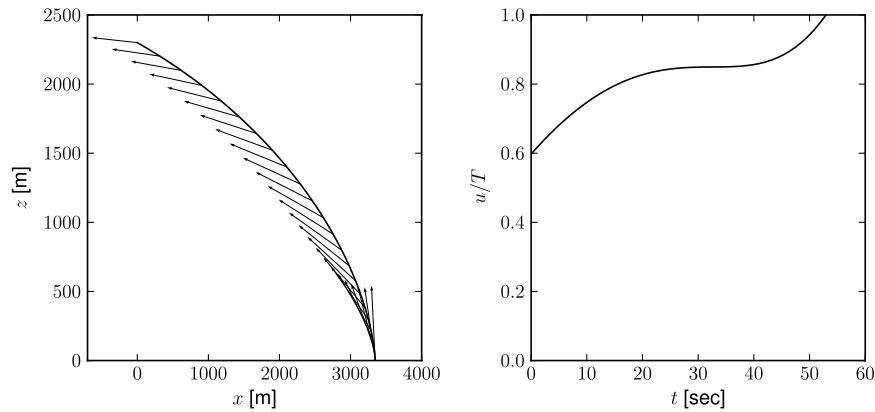


Fig. 14 Descent resulting from the proposed guidance scheme.

## VII. Conclusions

Planetary landings that maintain a constant optic flow throughout the descent are studied from the point of view of optimality. Some hints on the functional shape of the optimal pitch law during such descents is derived and a simple state feedback for the case of optimal minimum time is found. The mass penalty introduced to implement this bioinspired landing strategy is estimated to be of the order of 10% for a lunar high-gate/low-gate phase. Nonoptimal pitch laws are shown to lead to excessive mass consumptions and thus should be avoided. A constant-optic-flow guidance scheme based on a polynomial approximation of the horizontal spacecraft velocity is then proposed and proved to be a good approximation of the actual optimal constant-optic-flow descent, while only depending on the choice of two parameters: the descent duration and range.

## Acknowledgments

The authors wish to acknowledge Frank Ruffier, Stéphane Viollet, and Thibaut Raharijaona for their work carried out during the Ariadna project on neuromorphic computations of the optic flow, which inspired this research.

## References

- [1] Dickson, W., Straw, A., and Dickinson, M., "Integrative Model of *Drosophila* Flight," *AIAA Journal*, Vol. 46, No. 9, 2008, pp. 2150–2164. doi:10.2514/1.29862
- [2] Hyslop, A., and Humbert, J., "Autonomous Navigation in Three-Dimensional Urban Environments Using Wide-Field Integration of Optic Flow," *Journal of Guidance, Control, and Dynamics*, Vol. 33, No. 1, 2010, pp. 147–159. doi:10.2514/1.43778
- [3] Ruffier, F., and Franceschini, N., "Optic Flow Regulation: the Key to Aircraft Automatic Guidance," *Robotics and Autonomous Systems*, Vol. 50, No. 4, 2005, pp. 177–194. doi:10.1016/j.robot.2004.09.016
- [4] Jaroszewicz, A., Sibilski, K., Sibiliska, A., and Zyluk, A., "Biomimic Sensors Guided Flight Stability and Control for Flapping Wings Autonomous Micro Air Vehicle (Entomopter)," *AIAA Paper 2007-664*, Jan. 2007.
- [5] De Wagter, C., Bijnens, B., and Mulder, J., "Vision-Only Control of a Flapping MAV on Mars," *AIAA Paper 2007-6853*, Aug. 2007.
- [6] Janschek, K., Tchernykh, V., and Beck, M., "Performance Analysis for Visual Planetary Landing Navigation Using Optical Flow and DEM Matching," *AIAA Paper 2006-6706*, Aug. 2006.
- [7] Valette, F., Ruffier, F., and Viollet, S., "Neuromorphic Computation of Optic Flow Data," *ESA, TR Ariadna—08/6303b*, 2008.
- [8] Valette, F., Ruffier, F., Viollet, S., and Seidl, T., "Biomimetic Optic Flow Sensing Applied to a Lunar Landing Scenario," *2010 IEEE International Conference on Robotics and Automation (ICRA)*, IEEE, Piscataway, NJ, 2010, pp. 2253–2260.
- [9] Srinivasan, M., Zhang, S., Lehrer, M., and Collett, T., "Honeybee Navigation en Route to the Goal: Visual Flight Control and Odometry," *Journal of Experimental Biology*, Vol. 199, 1996, pp. 237–244.
- [10] Sostaric, R., and Rea, J., "Power Descent Guidance Methods for the Moon and Mars," *AIAA Paper 2005-6287*, Aug. 2005.
- [11] Mead, C., "Neuromorphic Electronic Systems," *Proceedings of the IEEE*, Vol. 78, No. 10, 1990, pp. 1629–1636. doi:10.1109/5.58356
- [12] Sarpeshkar, R., Salthouse, C., Sit, J.-J., Baker, M., Zhak, S., Lu, T.-T., Turicchia, L., and Balster, S., "An Ultra-Low-Power Programmable Analog Bionic Ear Processor," *IEEE Transactions on Biomedical Engineering*, Vol. 52, No. 4, Apr. 2005, pp. 711–727. doi:10.1109/TBME.2005.844043
- [13] Reichardt, W., *Movement Perception in Insects*, Academic Press, New York, 1968.
- [14] Ruffier, F., and Franceschini, N., "Octave, A Bioinspired Visuo-Motor Control System for The Guidance of Micro-Air Vehicles," *Proceedings of SPIE: The International Society for Optical Engineering*, Vol. 5119, 2003, pp. 1–12.
- [15] Franceschini, N., "Visual Guidance Based on Optic Flow: A Biorobotic Approach," *Journal of Physiology*, Vol. 98, Nos. 1–3, 2004, pp. 281–292. doi:10.1016/j.jphysparis.2004.06.002
- [16] Chahl, J., Srinivasan, M., and Zhang, S., "Landing Strategies in Honeybees and Applications to Uninhabited Airborne Vehicles," *International Journal of Robotics Research*, Vol. 23, No. 2, 2004, p. 101. doi:10.1177/0278364904041320
- [17] Franceschini, N., Pichon, J., and Blanes, C., "From Insect Vision to Robot Vision," *Philosophical Transactions of the Royal Society of London, Series B: Biological Sciences*, Vol. 337, No. 1281, 1992, pp. 283–294. doi:10.1098/rstb.1992.0106
- [18] Thakoor, S., Chahl, J., Srinivasan, M., Young, L., Werblin, F., Hine, B., et al., "Bioinspired Engineering of Exploration Systems for NASA and DoD," *Artificial Life*, Vol. 8, No. 4, 2002, pp. 357–369. doi:10.1162/106454602321202426
- [19] Parkes, S., Martin, I., and Dunstan, D., "Planet Surface Simulation with PANGU," *Eighth International Conference on Space Operations*, 2004.
- [20] Franceschini, N., Ruffier, F., and Serres, J., "A Bio-Inspired Flying Robot Sheds Light on Insect Piloting Abilities," *Current Biology*, Vol. 17, No. 4, 2007, pp. 329–335. doi:10.1016/j.cub.2006.12.032
- [21] Pontryagin, L., *The Mathematical Theory of Optimal Processes*, Wiley, New York, 1964.
- [22] Bryson, A., and Ho, Y., *Applied Optimal Control*, Wiley, New York, 1975.
- [23] Cheatham, D. C., Bennett, F. V., and Branch, T. M., "Apollo Lunar Module Landing Strategy," *Proceedings of the Apollo Lunar Landing Mission Symposium*, 1966, pp. 25–27.
- [24] Sims, J., and Flanagan, S., "Preliminary Design of Low-Thrust Interplanetary Missions," *AAS/AIAA Astrodynamics Specialist Conference*, AAS Paper 99-338, Girdwood, AK, Aug. 1999.
- [25] Chen, K., McConaghy, T., Landau, D., Longuski, J., and Aldrin, B., "Powered Earth-Mars Cypher with Three-Synodic-Period Repeat Time," *Journal of Spacecraft and Rockets*, Vol. 42, No. 5, Sept.–Oct. 2005, pp. 921–927. doi:10.2514/1.11610
- [26] Okutsu, M., Yam, C. H., and Longuski, J., "Low-Thrust Trajectories to Jupiter via Gravity Assists from Venus, Earth and Mars," *AIAA*

- Paper 2006-6745, Aug. 2006.
- [27] Parcher, D., and Sims, J., "Gravity-Assist Trajectories to Jupiter Using Nuclear Electric Propulsion Gravity-Assist Trajectories to Jupiter Using Nuclear Electric Propulsion," AAS/AIAA Astrodynamics Specialist Conference and Exhibit, AAS Paper 05-398, Lake Tahoe, CA, 2005.
- [28] Yam, C. H., "Design of Missions to the Outer Planets and Optimization of Low-Thrust, Gravity-Assist Trajectories Via Reduced Parametrization," Ph.D. Thesis, Purdue Univ., West Lafayette, IN, May 2008.
- [29] Yam, C., di Lorenzo, D., and Izzo, D., "Constrained Global Optimization of Low-Thrust Interplanetary Trajectories," *Proceedings of the Institution of Mechanical Engineers, Part G (Journal of Aerospace Engineering)* (to be published).